CHEPTER III

RESULTS AND DISCUSSION

3.1 PLA-based Multi-layered Films with PBS

3.1.1 PLA-*b*-PBS Copolymer Characterization

3.1.1.1 Structural Analysis

PLA and PBS prepolymers were prepared via the Steglich esterification as shown in Scheme 3.1. The successful product was traced with FTIR spectra (Figure 3.1). The characteristic peaks at 1754 cm^{-1} and 1713 cm^{-1} refer to carbonyl group of PLA and PBS prepolymer, respectively (Figure 3.1). In case of PLA-*b*-PBS copolymer, it shows both carbonyl groups of PLA at 1757 cm^{-1} and PBS at 1713 cm^{-1} (Figure 3.1). This indicates that PLA-*b*-PBS copolymer was successfully prepared.

Scheme 3.1

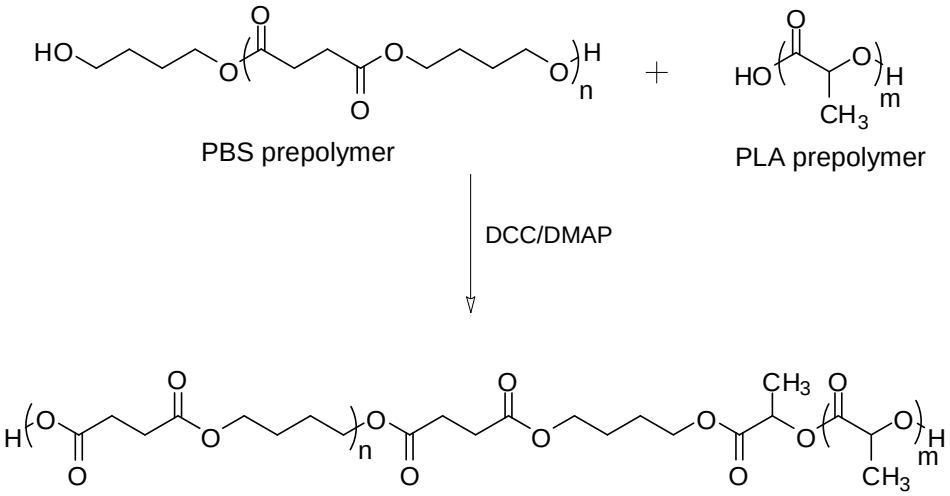

Poly(lactic acid-*b*-butylene succinate), PLA-*b*-PBS copolymer

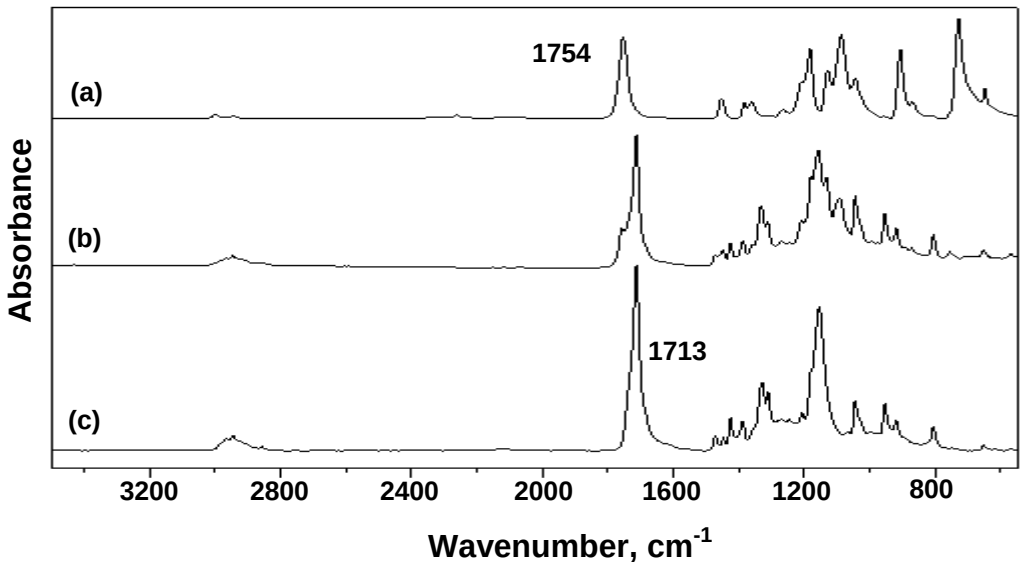

Figure 3.1 FTIR spectra of (a) PLA prepolymer, (b) PLA-*b*-PBS copolymer, and (c) PBS prepolymer.

^{1}H and ^{13}C NMR of PLA-*b*-PBS copolymer are shown in Figure 3.2. In order to clarify the structure of PLA-*b*-PBS copolymer, heteronuclear multiple bond correlation (HMBC) 2D NMR was used. This mode of NMR indicates the correlation between the carbon and proton via multiple bonds. The result shows one correlation between PLA and PBS units as indicated in the structure in Figure 3.3. The correlation was found between methyl group of PLA unit (at 1.57, 16.75 ppm) and methylene group of PBS unit (at 1.69, 25.34 ppm).

In addition, the number-average molecular weight ($M_{n\text{-}NMR}$) of PLA-*b*-PBS copolymer (3904 g/mole) was calculated according to equation 1 by using quantitative ^{1}H-NMR analysis (You *et al.*, 2004).

$$M_{n\text{-}NMR} = \left(\frac{I_{1.57}/3}{I_{3.67}/2} \times 72\right) + \left(\frac{I_{2.61}/4}{I_{3.67}/2} \times 172\right) \qquad \text{(Eq. 1)}$$

where $I_{1.57}$ is the integral value of the peak at δ_H = 1.57 (3H, d, -O-CH(C**H**$_3$)-) in PLA. $I_{2.61}$ and $I_{3.67}$ are the integral value of the peaks at δ_H = 2.61 (4H, s, -(C=O)-C**H**$_2$-) and 3.67 (2H, s, HO-C**H**$_2$-CH$_2$-) in PBS. 72 and 172 are the molecular weight (g/mole) of PLA and PBS unit, respectively.

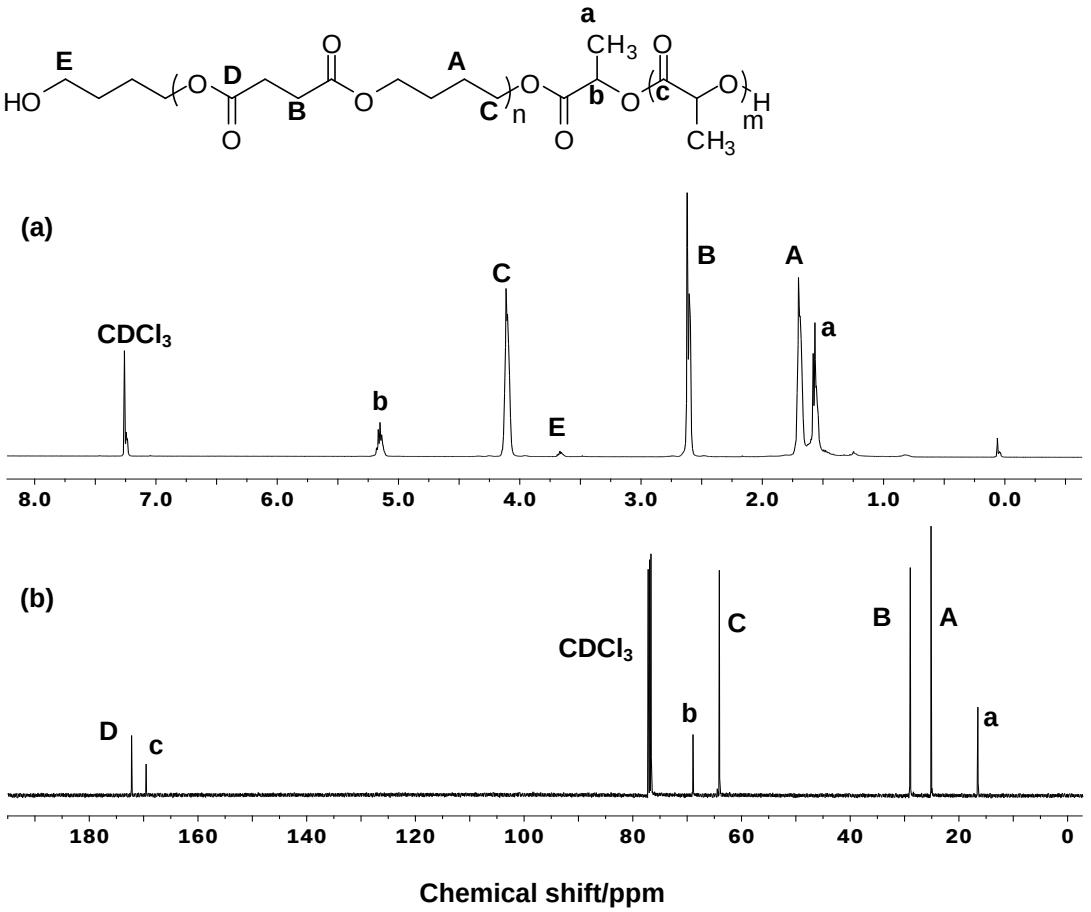

Figure 3.2 (a) ^{1}H and (b) ^{13}C NMR of PLA-*b*-PBS copolymer.

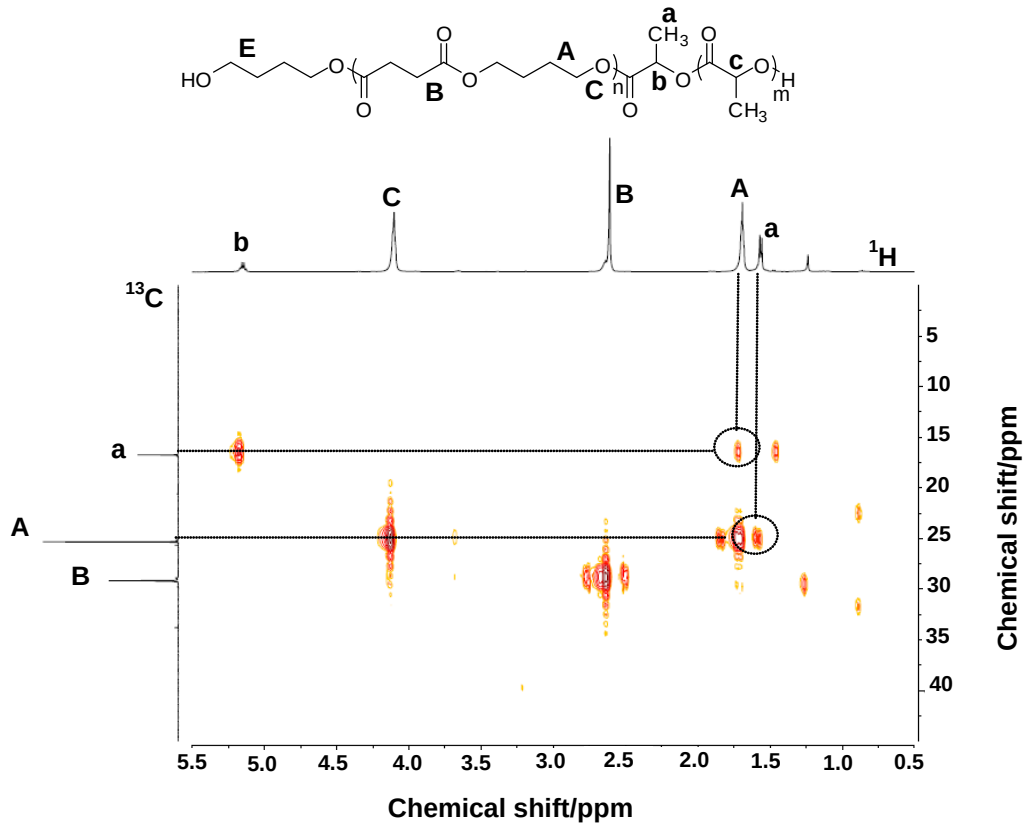

Figure 3.3. ^{1}H-^{13}C HMBC 2D NMR spectrum of PLA-*b*-PBS copolymer.

3.1.1.2 Thermal Analysis

As shown in Figure 3.4, PLA-*b*-PBS block copolymer shows the melting points of PBS and PLA chains around 110.7 $^{\circ}$C and 151.4 $^{\circ}$C, respectively. The intensity of endothermic peak of PLA block is relatively low, compared to that of PBS block. This might be the effect of slow crystallization of PLA although it covalently bonds with high crystalline PBS block.

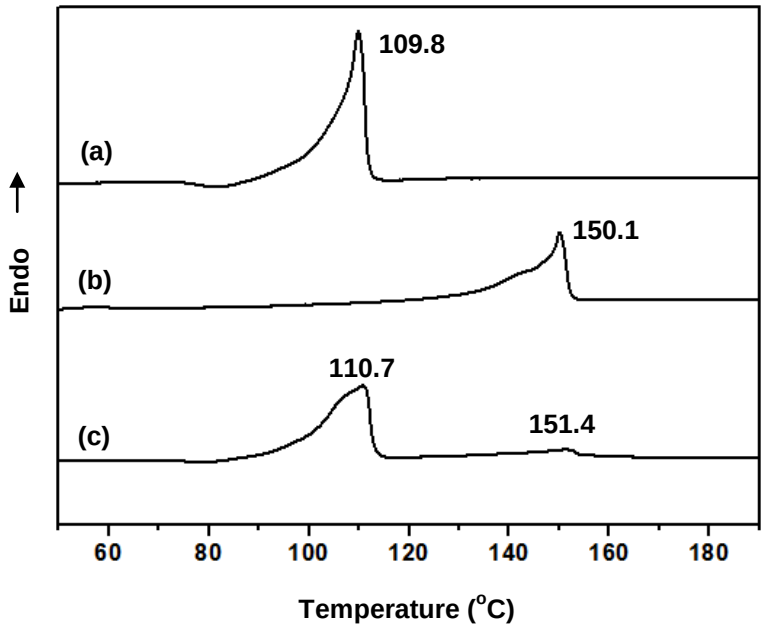

Figure 3.4 DSC curves of (a) PBS prepolymer, (b) PLA prepolymer, and (c) PLA-*b*-PBS copolymer.

3.1.1.3 Spherulite Study

The crystallization in macroscopic scale of PLA-*b*-PBS copolymer can be observed by using an optical microscope. In general, the highly crystalline polymer melt shows spherulite formation during cooling down temperature from the crystallization temperature to the glass transition temperature. Here, the crystallization behavior of PLA-*b*-PBS copolymer was observed at isothermal thermal temperature of 70 °C which is close to the onset of the crystallization temperature of PBS. Figure 3.5 presents the spherulite morphologies of PLA-*b*-PBS copolymer. At 135 s, it shows that the average radius of the spherulites is about 54 μm with the growth spherulites rate about 0.8 μm/s.

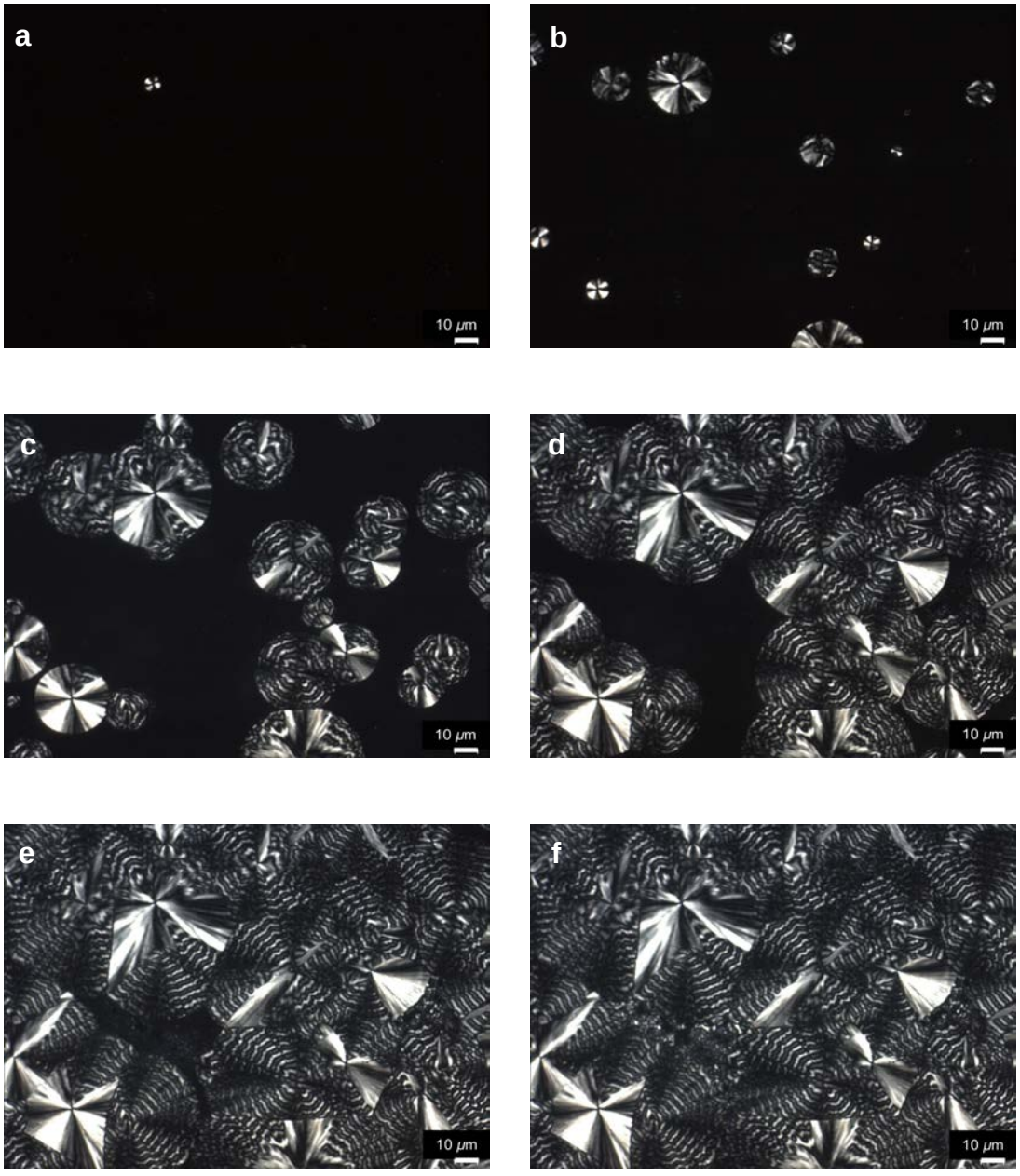

Figure 3.5 Polarizing optical micrographs for PLA-*b*-PBS at isothermal temperature (70 °C): (a) 10 sec, (b) 35 sec, (c) 60 s, (d) 85 sec, (e) 110 sec, and (f) 135 sec.

3.1.2 Characterizations of PLA/PBS/PLA Multi-layered Films

3.1.2.1 Compatibility Study

The efficiency of PLA-*b*-PBS copolymer can evaluate from the compatibility of PLA/PBS/PLA multi-layered films containing PLA-*b*-PBS copolymer as a compatibilizer. Figure 3.6 ((A), (B), (C), (D), (E)) represents morphology of the multi-layered film with 0, 0.5, 1, 3, 5 phr of copolymer, respectively. It is clear that the addition of copolymer shows the improvement of compatibility between PLA and PBS phases as identified by decreasing of the white line between two-phase polymers. This white line refers to interphase which is the boundary between two-phase polymers. In other words, the PLA-*b*-PBS copolymer can increase interfacial adhesion between PLA and PBS polymers.

In order to investigate whether PLA-*b*-PBS copolymer interact with PLA and PBS, total correlation spectroscopy (TOCSY) 2D NMR technique was applied. This technique determines the correlation between the proton and proton via multiple bonds. Figure 3.7B represents the PLA/PBS/PLA multi-layered film containing PLA-*b*-PBS copolymer. The correlation at 1.70 ppm (C**H**$_2$-A of PBS) and at 5.17 ppm (C**H**-b of PLA) indicates the interaction of PLA, PBS, and PLA-b-PBS copolymer. It should be noted that the result of PLA/PBS/PLA multi-layered film without PLA-*b*-PBS copolymer was not found any correlation in that region (Figure 3.7A).

GPC technique was also used to confirm the number of component in multi-layered film containing copolymer. It should be mentioned that Figure 3.8c is the mixture of PLA/PBS/PLA multi-layered film and PLA-*b*-PBS copolymer in the solvent of HPLC-grade chloroform ($CHCl_3$), which 2 peaks at 25.762 min (PLA-PBS phases) and 31.876 min (PLA-*b*-PBS) were observed, while Figure 3.8b is the PLA/PBS containing PLA-*b*-PBS/PLA

multi-layered film passed extruder. The observation of one peak at 25.807 min in Figure 3.8b implied that PLA-PBS phases and PLA-*b*-PBS copolymer after processing have one component in the system. In other word, some chemical bonds between them were occurred.

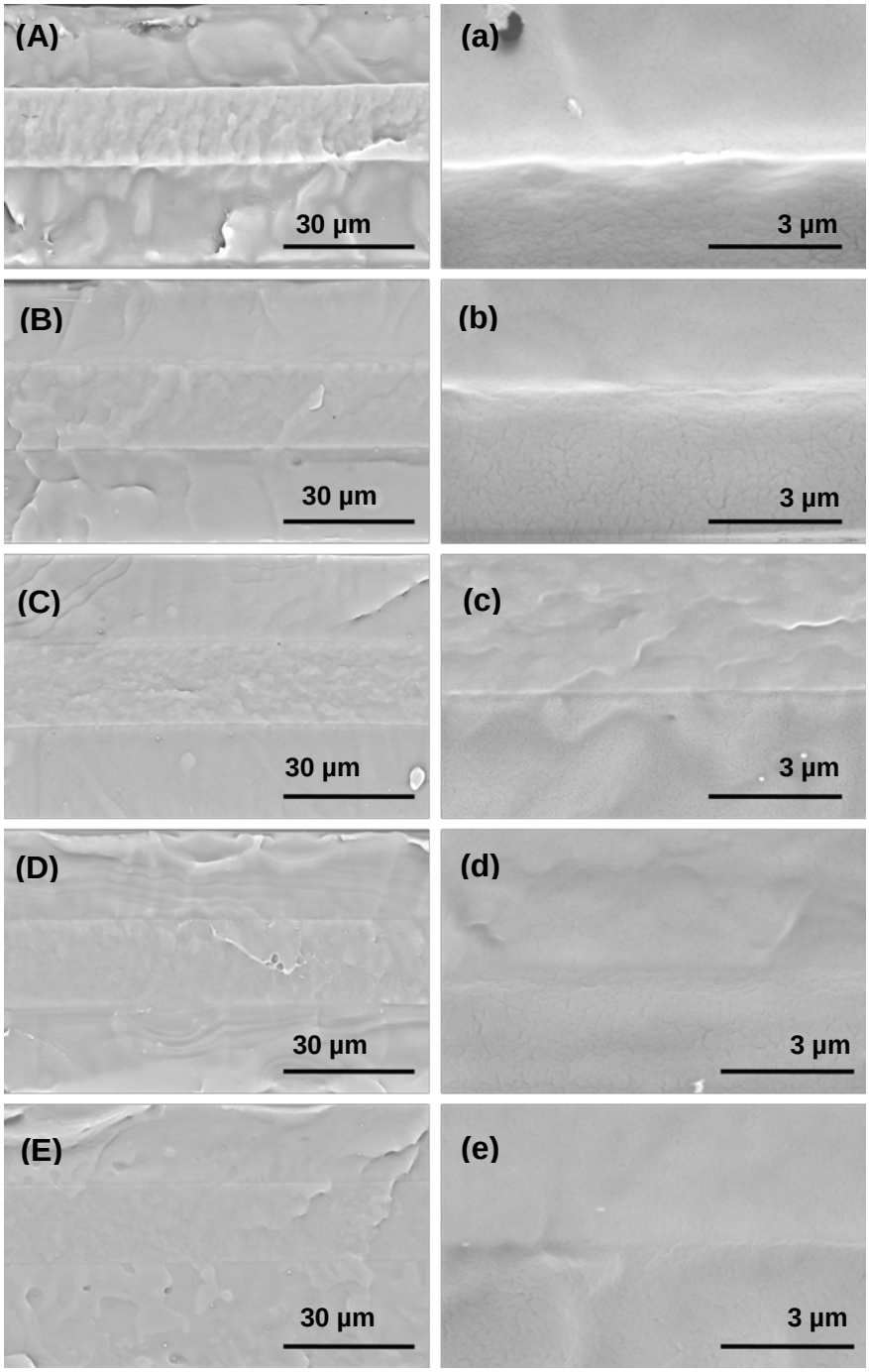

Figure 3.6 SEM images of PLA/PBS/PLA multi-layered films with PLA-*b*-PBS copolymer (A,a) 0 phr, (B,b) 0.5 phr, (C,c) 1.0 phr, (D,d) 3.0 phr, and (E,e) 5.0 phr.

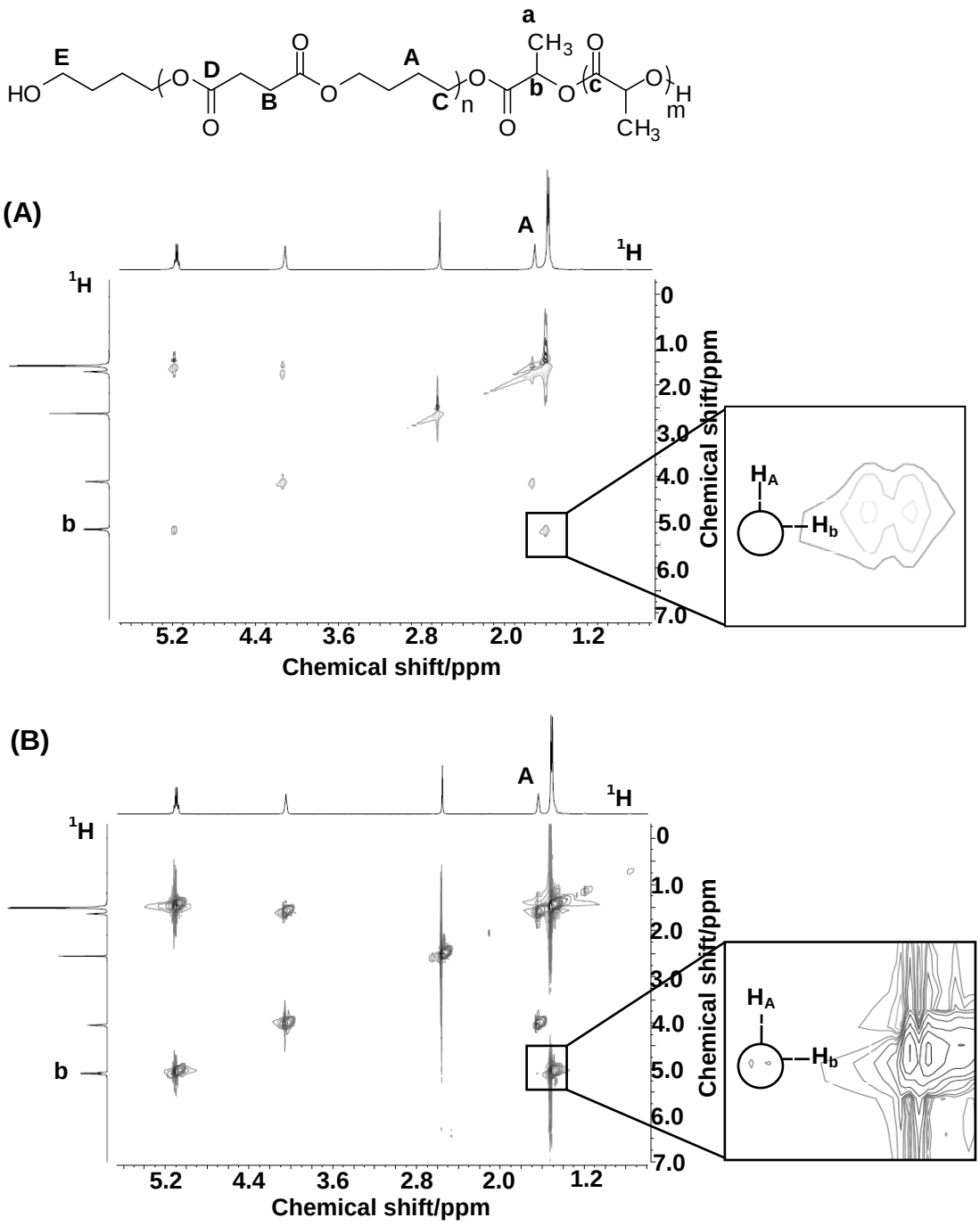

Figure 3.7 ^{1}H-^{1}H TOCSY 2D NMR spectra of (A) PLA/PBS/PLA and (B) PLA/PBS+PLA-*b*-PBS5/PLA multi-layered films.

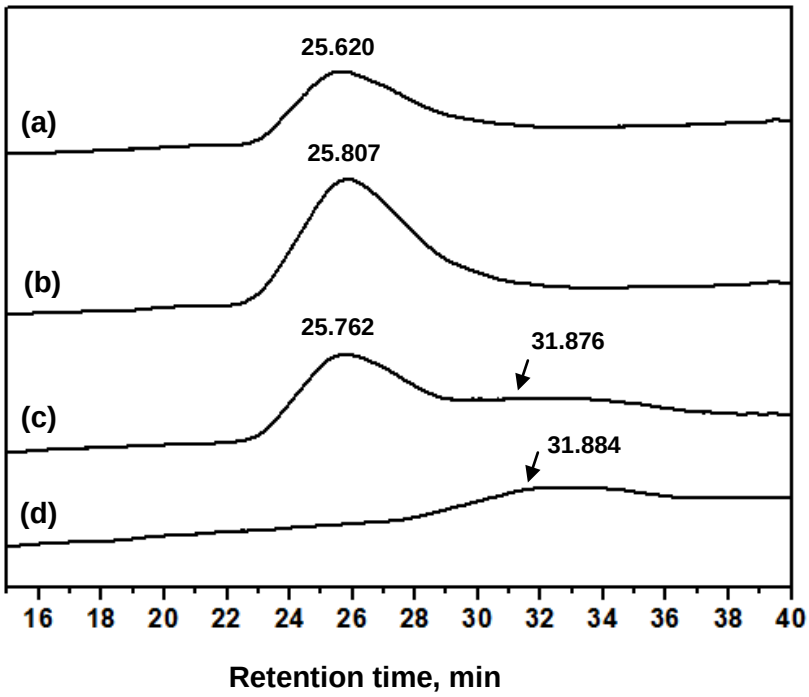

Figure 3.8 GPC chromatogram of (a) PLA/PBS/PLA film, (b) PLA/PBS+PLA-*b*-PBS5/PLA film, (c) PLA/PBS/PLA mixing with PLA-*b*-PBS copolymer 5 phr, and (d) PLA-*b*-PBS copolymer.

3.1.2.2 Thermal Properties and Crystallization Behavior

Thermal properties and crystallization behavior of the multi-layered films were evaluated using DSC (Table 3.1). The PLA/PBS/PLA and PLA/PBS+PLA-*b*-PBS/PLA multi-layered films show the decrease in T_g with an increase of PLA-*b*-PBS. In other words, the ease of chain mobility occurs when PBS phase contained PLA-*b*-PBS. This leads to an understanding that PLA-*b*-PBS plays the role as compatibilizer for PLA and PBS. The compatibility of PBS and PLA in the multi-layered films also leads to the decrease of T_c as well as the increase of degree of the crystallinity (X_c).

Table 3.1 Thermal properties and crystallinity of PLA/PBS/PLA multi-layered films

Multi-layered film	$T_{g,PLA}$ (^{o}C)	$T_{m,PBS}$ (^{o}C)	$T_{m,PLA}$ (^{o}C)	$T_{c,PLA}$ (^{o}C)	X_c (%)
PLA/PLA/PLA	57.7	-	154.3	101.4	~0
PLA/PBS/PLA	55.3	109.0	152.7	85.8	8.07
PLA/PBS+PLA-b-PBS0.5/PLA	54.0	109.2	153.1	85.5	8.52
PLA/PBS+PLA-b-PBS1/PLA	53.5	109.0	152.0	85.1	9.11
PLA/PBS+PLA-b-PBS3/PLA	52.6	108.6	152.6	84.4	10.72
PLA/PBS+PLA-b-PBS5/PLA	52.1	109.1	152.3	84.2	12.01

3.1.2.3 Mechanical Properties

Figure 3.9 illustrates the mechanical properties of the multi-layered films. The result shows that PLA/PBS/PLA multi-layered film is decreased in tensile strength compared with the PLA/PLA/PLA film. This might be due to the phase separation between the two phases of the different polymers. However, the tensile strength of film is increased when containing PLA-*b*-PBS copolymer for 0.5 phr. In addition, it is clear from this table that the elongation at break is obviously increased for the multi-layered films containing PLA-*b*-PBS copolymer. This might be due to the role of PLA-*b*-PBS copolymer.

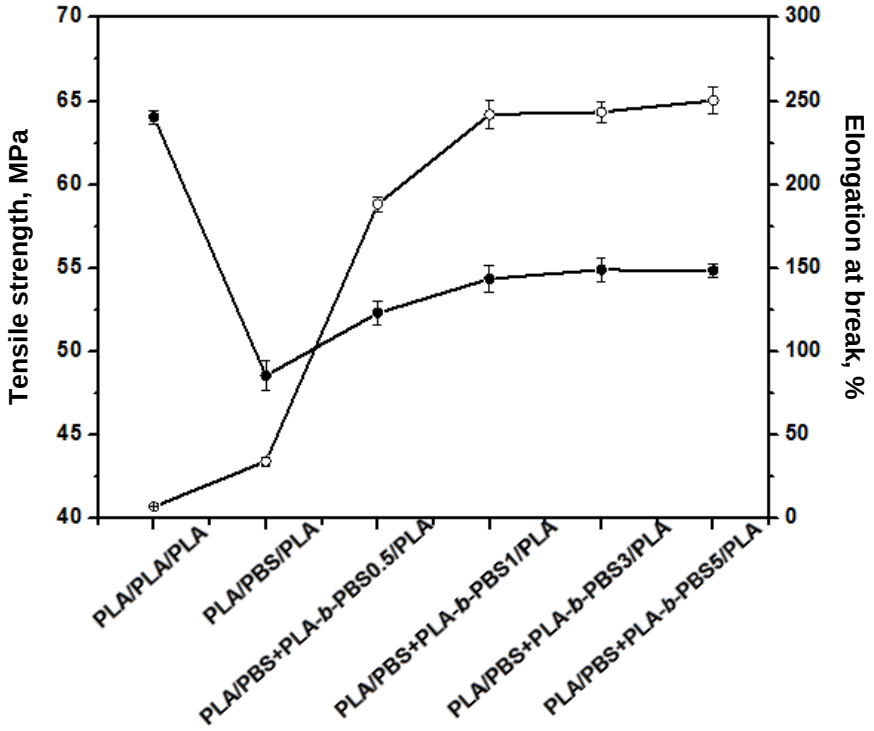

Figure 3.9 Tensile strength and elongation at break of PLA/PBS/PLA multi-layered films containing PLA-*b*-PBS copolymer.

3.1.2.4 Oxygen Permeability

As seen in Figure 3.10, the oxygen permeability of PLA/PLA/ PLA and PBS/PBS/PBS multi-layered films is about 20.0 and 28.5 cm^3 mm m^{-2} day^{-1} atm^{-1}, respectively. Unexpectedly, when PLA and PBS were formed together (PLA/PBS/PLA multi-layered film), the oxygen permeability is decreased (18.4 cm^3 mm m^{-2} day^{-1} atm^{-1}) less than their individual values. This suggests that PLA and PBS are synergistic property in term of oxygen permeability.

The fact that crystallinity can be affected on oxygen permeability.[11] As shown in Table 3.1 PLA/PBS/PLA multi-layered film shows an increase in crystallinity (X_c)

from ~0 % to 8.07 % compared with the PLA/PLA/PLA film. It should be noted that this reflects the packing structure of polymer chain resulting in obstructing O_2 molecules. In case of PLA/PBS+PLA-*b*-PBS/PLA multi-layered films, it slightly increases in crystallinity resulting in slightly decrease of oxygen permeability.

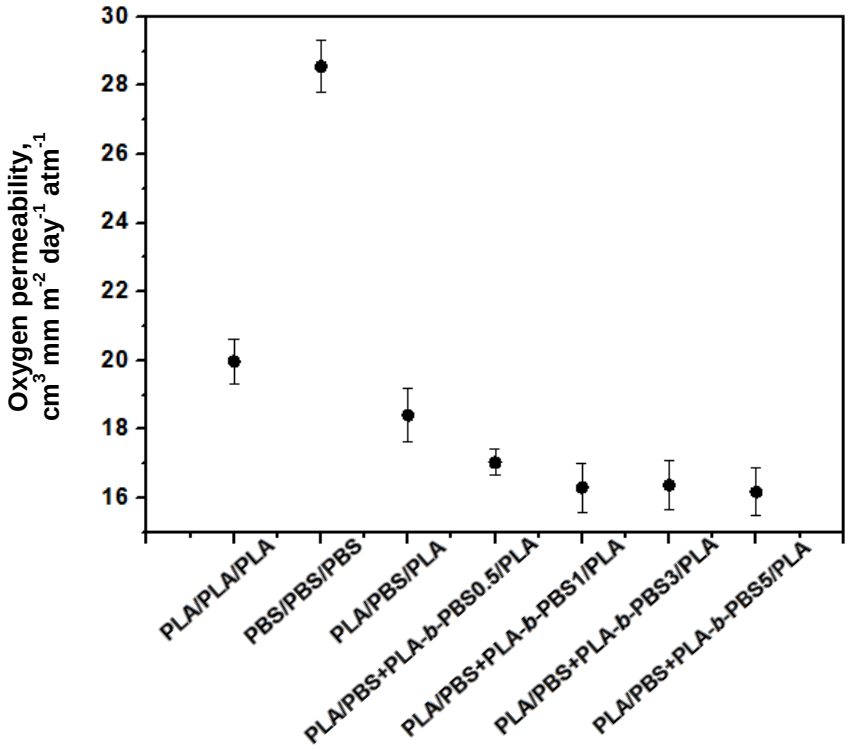

Figure 3.10 Oxygen permeability of PLA/PBS/PLA multi-layered films.

Moreover, XRD analysis was used to characterize the crystallinity pattern of the multi-layered films. The result shows that PBS can induce the crystallization of PLA (2Θ = 15.8°) as seen in Figure 3.11c.

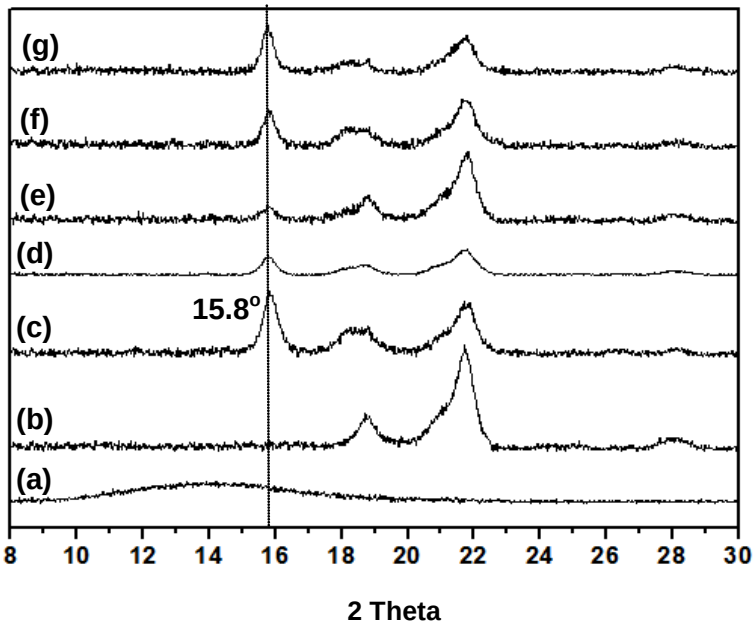

Figure 3.11 XRD pattern of (a) PLA/PLA/PLA, (b) PBS/PBS/PBS, (c) PLA/PBS/PLA, (d) PLA/PBS+PLA-*b*-PBS0.5/PLA, (e) PLA/PBS+PLA-*b*-PBS1/ PLA, (f) PLA/PBS+PLA-*b*-PBS3/PLA, (g) PLA/PBS+PLA-*b*-PBS5/PLA.

3.1.3 Vacuum Applications

Figure 3.12 illustrates PLA/PBS+PLA-*b*-PBS1/PLA multi-layered film in vacuum applications.

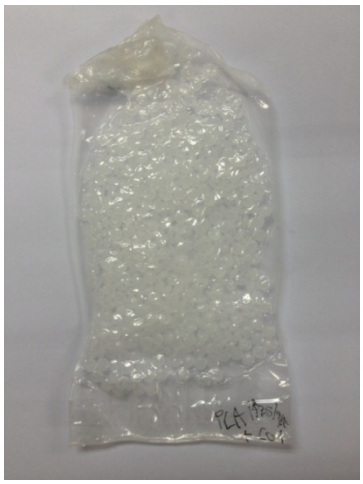

Figure 3.12 Vacuum packaging of PLA/PBS/PLA multi-layered film.

3.1.4 Conclusions

The present work demonstrated the PLA/PBS/PLA multi-layered films. By simply copolymerization PLA and PBS with conjugating reaction, PLA-*b*-PBS can be obtained. The addition of PLA-*b*-PBS in PLA/PBS/PLA multi-layered films clarified to us that PLA-*b*-PBS played an important role as compatibility for PLA and PBS. An increased of PLA-*b*-PBS content, in the range of 3-5 phr, led to an increase of film elongation at break for 5-8 times. The compatibility of PLA and PBS also initiated the change in packing structure of PLA as confirmed by the decrease in T_g and T_c as well as the increase in degree of crystallinity. Moreover, oxygen permeability of PLA/PBS/PLA and PLA/PBS+PLA-*b*-PBS/PLA multi-layered films was improved due to the crystallinity factor.

3.2 PLA-based Multi-layered Films with TPS

3.2.1 TPS Characterizations

3.2.1.1 Structural Analysis

The FT-IR spectrum of TPS is represented in Figure 3.13b. The board peak referred to hydroxyl group of pyranose ring in starch molecules shifts to lower wavenumber from at 3395 cm^{-1} to at 3299 cm^{-1}. It indicates that the strong hydrogen bonds in starch molecules become weaker which might be an impact of glycerol penetration in polysaccharide chains obstructing the packing structure. Additionally, the intensity of characteristic peaks in the range of 1200-1100 cm^{-1}, assigned to C-O-C stretching, decrease obviously which points out that chain scission of polysaccharide could occur under extrusion process, and consequently, destroy glycosidic linkage.

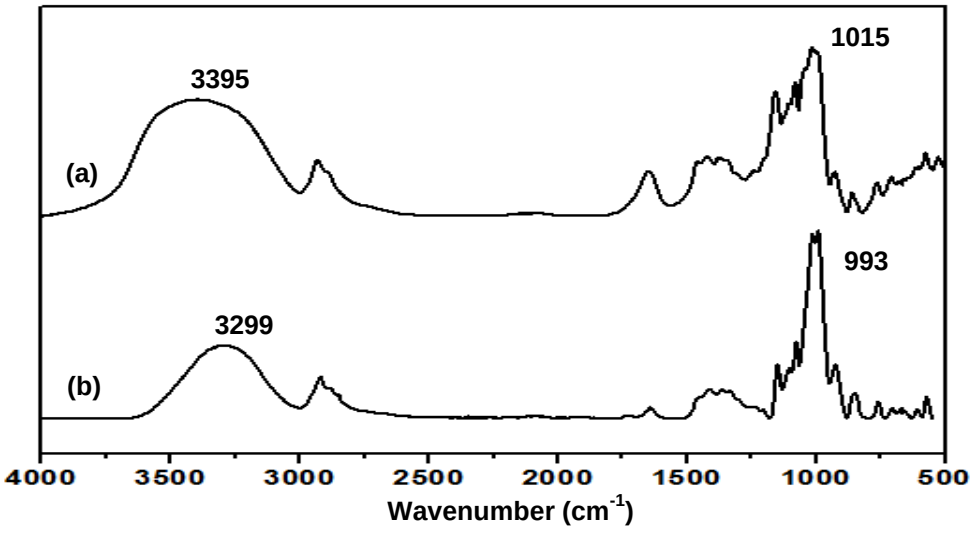

Figure 3.13 FT-IR spectra of (a) dry starch, and (b) TPS.

3.2.1.2 Thermal Analysis

The non-isothermal analysis by DSC technique was applied to study the thermal properties of TPS obtained. Normally, dry starch has high melting temperature (T_m) due to its degradation temperature (T_d) around ~220-230 $^{\circ}C$, resulting in degradation before melting. Although TPS was formed, there was no any endothermic peak observed (Figure 3.14).

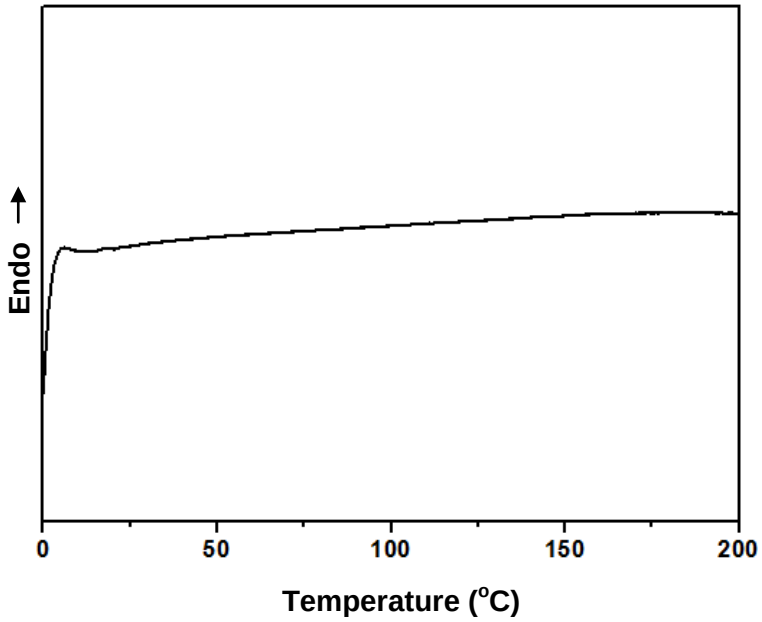

Figure 3.14 DSC curve of TPS.

3.2.1.3 Spherulite Study

In order to follow crystalline morphology change of TPS, the polarizing optical microscope was applied. In general, starch is highly crystalline material with high melting point (~230 °C) and it always shows a characteristic "maltese cross" under polarized

light as shown in Figure 3.15a. After extrusion process (Figure 3.15b), the maltese crosses are mostly disappeared in TPS due to the extremely shear force and heat during process which breaks the highly packing structure of starch molecules. Moreover, the glycerol addition also limits the stacking of shorten polysaccharide chains to reform ordered packing.

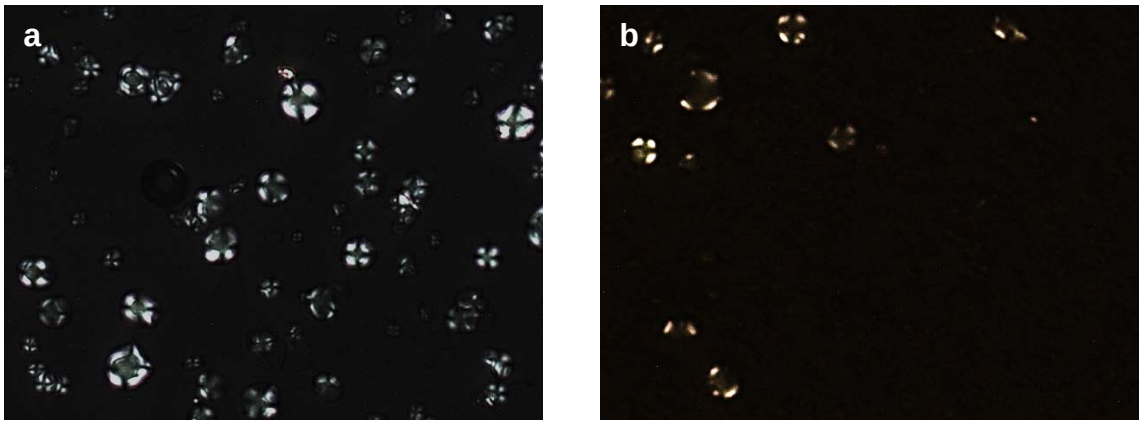

Figure 3.15 Polarizing optical micrographs of (a) tapioca starch and (b) TPS.

3.2.2 Characterizations of PLA/TPS/PLA Multi-layered Films

3.2.2.1 Thermal Properties

Thermal properties of the multi-layered film were studied by non-isothermal temperature profile using DSC technique (Table 3.2). The neat PLA multi-layered film shows the glass transition temperature (T_g), crystallization temperature (T_c), and melting temperature (T_m) at 57 $^{\circ}$C, 101 $^{\circ}$C, and 154 $^{\circ}$C, respectively. The percent of crystallinity (X_c) was around 0 %. In term of TPS, it does not show T_g, T_c, and T_m during non-isothermal study (Guinault *et al.*, 2010).

After the addition of TPS into the PLA-based multi-layered films, it was found that T_g, T_c, and T_m decreased. As T_g represents the mobility of the polymer chains, the lower T_g means the polymer chain can be moved easier, in other word, chain mobility increases when TPS was added into the system. This might be due to the glycerol in TPS can cause plasticization. The shift of the T_c to the lower temperature means that the system allows crystallization easier as evidenced from increasing of crystallinity (X_c). These results implied that TPS can act as plasticizer and nucleating agent.

Table 3.2 Thermal properties of PLA/TPS/PLA multi-layered films

Multi-layered film	$T_{g,PLA}$ (^{o}C)	$T_{m,PLA}$ (^{o}C)	$T_{c,PLA}$ (^{o}C)	X_c (%)
PLA/PLA/PLA	57.7	154.3	101.4	~0
PLA/TPS50/PLA	54.0	147.9	94.6	1.32
PLA/TPS60/PLA	54.6	147.3	95.8	3.45
PLA/TPS70/PLA	54.0	148.8	95.4	4.13
PLA/TPS80/PLA	54.8	148.4	96.2	4.29
PLA/TPS90/PLA	54.2	147.8	95.4	5.50
PLA/TPS100/PLA	53.2	148.1	94.7	6.53

3.2.2.2 Mechanical Properties

Table 3.3 illustrates the mechanical properties of the multi-layered films. The tensile strength and young's modulus of PLA/TPS/PLA multi-layered films decreased compared with the PLA/PLA/PLA multi-layered film. This might be due to the

phase separation between PLA and TPS as seen from SEM images (Figure 3.16). However, the elongation at break slightly increased until the core layer is the blend between TPS 90 % and PLA 10 %. For PLA/TPS100/PLA multi-layered film, it is obviously increased in elongation at break because it is more homogeneous in core layer (TPS) (Figure 3.16(f)).

Table 3.3 Mechanical properties of PLA/TPS/PLA multi-layered films

Multi-layered film	Tensile strength (MPa)	Young's modulus (GPa)	Elongation at break (%)
PLA/PLA/PLA	64.03±0.4	3.47±0.1	7.24±0.2
PLA/TPS50/PLA	44.91±0.3	2.15±0.1	10.28±0.9
PLA/TPS60/PLA	40.05±0.6	2.13±0.04	14.16±0.5
PLA/TPS70/PLA	37.56±0.9	1.91±0.05	14.19±0.3
PLA/TPS80/PLA	35.57±0.8	1.77±0.04	14.95±0.7
PLA/TPS90/PLA	33.83±0.9	2.07±0.03	16.60±1.0
PLA/TPS100/PLA	32.58±0.9	2.04±0.03	26.66±0.6

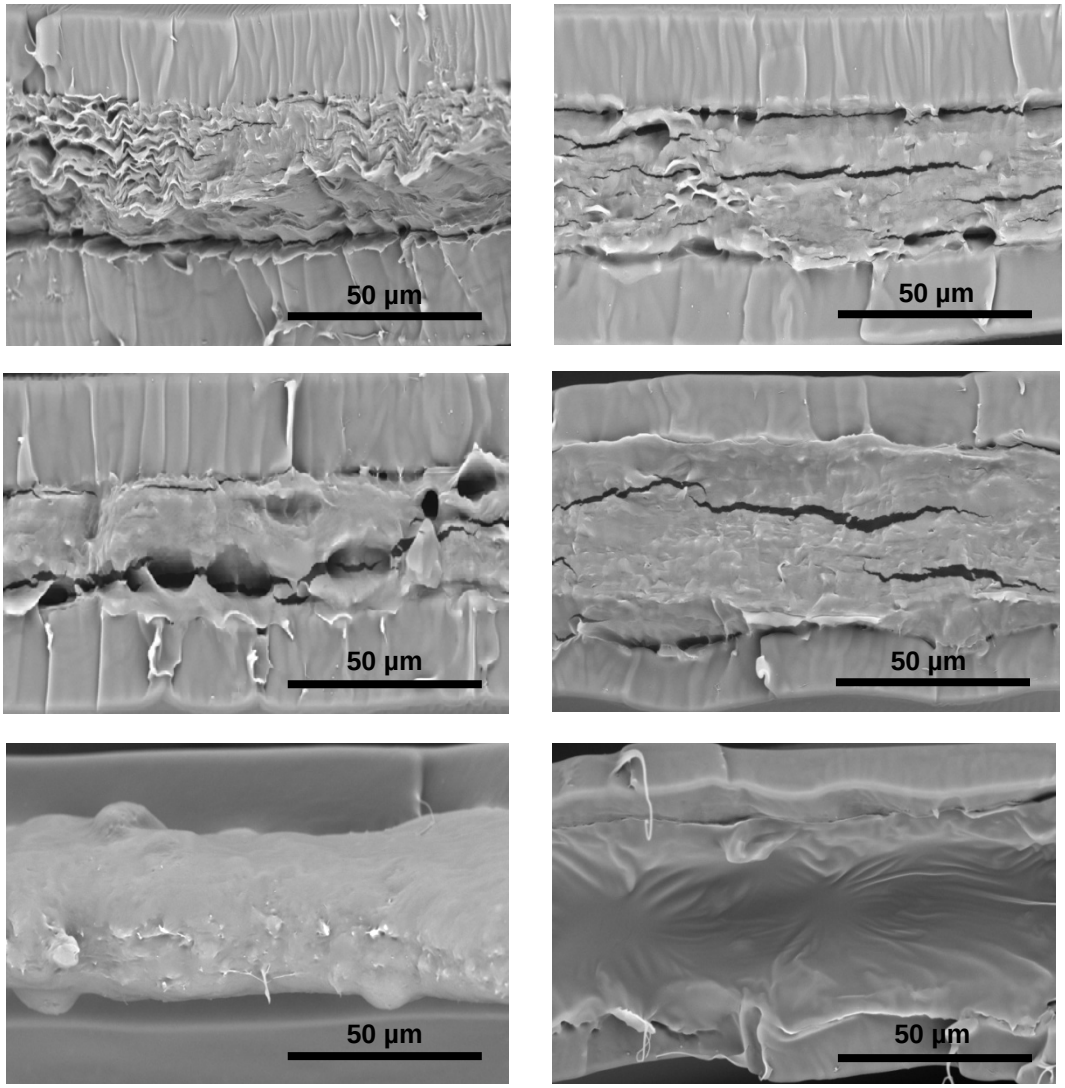

Figure 3.16. SEM images of multi-layered films: (a) PLA/TPS50/PLA, (b) PLA/TPS60/PLA, (c) PLA/TPS70/PLA, (d) PLA/TPS80/PLA, (e) PLA/TPS90/PLA, and (f) PLA/TPS100/PLA.

3.2.2.3 Water Absorption

In general, PLA is a hydrophobic polymer while starch is a hydrophilic polymer due to an abundance of hydroxyl groups. Figure 3.17 illustrates the percent of water absorption of the multi-layered films submerged in water chamber at 25 $^{\circ}$C. The result

shows that an increase of TPS content in PLA-based multi-layered films led to an increase of amount of water containing in the films. For 100 % TPS in the multi-layered film (PLA/TPS100/PLA), it can take up the water inside the films from 0.3 % to 115 % compared with neat PLA film (PLA/PLA/PLA). It indicated that the TPS was the major effect on the water absorption of the multi-layered films. All of the multi-layered films containing TPS were constant when the time passed for 6 days.

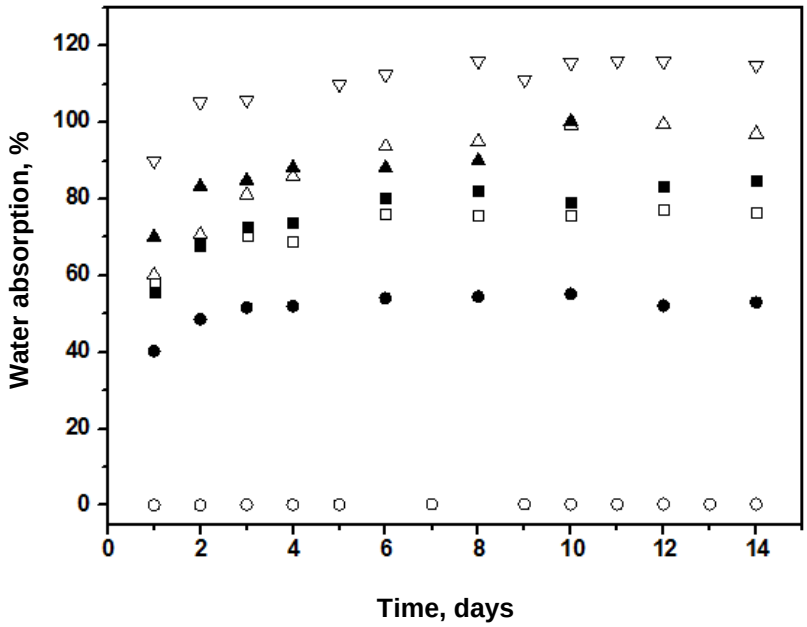

Figure 3.17 Effect of moisture content in the PLA/TPS/PLA multi-layered films on water absorption behavior: (○) PLA/PLA/PLA, (●) PLA/TPS50/PLA, (□) PLA/TPS60/PLA, (■) PLA/TPS70/PLA, (△) PLA/TPS80/PLA, (▲) PLA/TPS 90/PLA, and (▽) PLA/TPS100/PLA.

3.2.2.4 Oxygen Permeability

The oxygen permeability of multi-layered films was presented in Figure 3.18. Oxygen permeability of neat PLA film is about 20 cm^3 mm m^{-2} day^{-1} atm^{-1}. When TPS was combined into multi-layered films, the oxygen permeability decreased. As TPS can form H-bonding between polymer chains, this might result in tight packing structure obstructed O_2 molecules passing through the films. Another factor affected on oxygen permeability is crystallinity.[11] As shown in Table 3.2, it was found that an increase in crystallinity was observed with increasing TPS content.

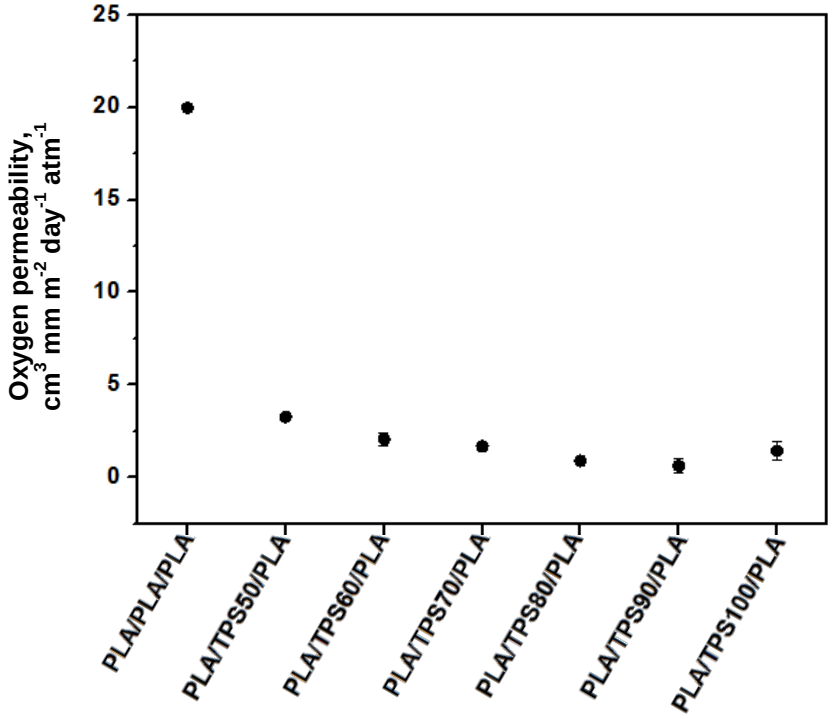

Figure 3.18 Oxygen permeability of PLA/TPS/PLA multi-layered films.

3.2.3 Conclusions

The present work proposed the biodegradable multi-layered films between PLA and TPS. The TPS and TPS blended with PLA were added in the core layer of PLA-based multi-layered films. The elongation at break was improved when the 100 % TPS content in core layer (PLA/TPS100/PLA) was performed. However, the water absorption obviously increased as the content of TPS increased. Furthermore, the addition of TPS into PLA-based multi-layered film resulted in a decrease of oxygen permeability.